Available online at www.sciencedirect.com
SCIENCE DIRECT®
International Journal of Heat and Mass Transfer 49 (2006) 3728–3745
International Journal of HEAT and MASS TRANSFER
www.elsevier.com/locate/ijhmt

Intense heat simulation studies on window of high density liquid metal spallation target module for accelerator driven systems

V. Mantha [a], R. Chaudhary [a], S. Pal [a], S. Gourai [a], P.S.S. Murthy [a], S.N. Sahasrabudhe [a], G. Biswas [b], A.K. Das [a], P. Satyamurthy [a,*]

[a] *Laser and Plasma Technology Division, Bhabha Atomic Research Center, Trombay, Mumbai 400085, India*
[b] *Department of Mechanical Engineering, Indian Institute of Technology, Kanpur 208016, India*

Received 24 June 2005; received in revised form 20 December 2005
Available online 16 June 2006

Abstract

The design of the spallation target system for accelerator driven systems requires a detailed understanding of the thermal-hydraulic issues involved as intense heat is deposited both in the window as well as in the target. Removal of heat from the window is a big thermal-hydraulic challenge. A lead–bismuth eutectic (LBE) experimental flow loop is currently being designed (1:1 size of an actual target both in terms of geometry and flow rate) to study thermal-hydraulics of the target system. It is proposed to simulate the proton beam heating of the window with a plasma heat source. In this paper, flow simulation studies have been performed for different target geometries and flow configurations with different window materials, which are proposed for the above said experimental loop. Optimal values of window geometry and flow configurations including the thermal loads the window experiences have been arrived at along with the required parameters for the plasma torch. The plasma torch has been tested and found to be suitable for simulation of proton beam heating in LBE loop to be set up.

Keywords: Accelerator driven systems (ADS); Lead–bismuth eutectic (LBE); Neutron spallation target; Plasma torch-heat simulator; CFD; Window

1. Introduction

Recently, studies have been taken up in world's leading nuclear research institutes to develop accelerator driven sub-critical reactor systems (ADS) [1]. The ADS system utilizes the neutrons produced in a spallation (spallation corresponds to the nuclear reaction mechanism by which high energy projectile pulls out of the target nucleus some nucleons and/or light particles, leaving a residual nucleus known as spallation product) target by a high-energy proton beam to drive a blanket assembly containing both fissionable fuel and radioactive waste. The spallation target is ideally conceived to be high Z material and heavy density liquid metals like lead; lead–bismuth eutectic (LBE) fit the requirement extremely well. The following are the attractive features of ADS: (1) extremely high level of inherent safety, (2) minimum production of long lived wastes and ability to transmute nuclear waste generated in normal reactors, (3) high resistance to proliferation and (4) more efficient use of abundantly available natural fuel (^{232}Th). The novel feature of ADS is the presence of a neutron spallation target in the core of the reactor, which always operates under sub-critical conditions. A proton beam (energy: ~1 GeV and current: ~few mA) interacts with the target, which is located in the core and produces spallation neutrons that diffuse into the reactor and drive the reactor. Two critical operating conditions for the ADS spallation target are: very high volumetric heat deposition rate (few kW/cm^3) and irradiation measured in terms of displacements per atom (DPA), by high fluence of energetic protons as well as neutrons (~100 DPA/year). To overcome this problem, liquid metal targets consisting of lead and lead–bismuth eutectic (LBE) have been proposed [2]. Currently two types of generic target modules, i.e., window and windowless concepts have

* Corresponding author. Tel.: +91 22 255 93822; fax: +91 22 255 05151.
E-mail address: lmmhd@barc.gov.in (P. Satyamurthy).

0017-9310/$ - see front matter © 2006 Published by Elsevier Ltd.
doi:10.1016/j.ijheatmasstransfer.2005.12.020

Nomenclature

C_p	specific heat, J/kg K
C_μ	constant in the turbulence model
$C_{1\varepsilon}$	constant in the turbulence model
$C_{2\varepsilon}$	constant in the turbulence model
G	turbulent kinetic energy source term
g_z	component of acceleration due to gravity, m/s^2
k_m	molecular thermal conductivity, W/m K
k	turbulent kinetic energy per unit mass, m^2/s^2
P	static pressure, N/m^2
r	radial coordinate, m
S_k	net turbulent kinetic energy source term
T	temperature, K
t	time, s
u_r, u_z	components of the velocity vectors in the r, z directions, m/s
z	axial coordinate, m

Greek symbols

β	coefficient of volumetric expansion, K^{-1}
ε	turbulent kinetic energy dissipation rate per unit mass, m^2/s^3
Γ_k	effective conductivity, W/m K
μ_e	effective viscosity, N s/m^2
μ_m	molecular viscosity, N s/m^2
μ_t	turbulent viscosity, N s/m^2
ρ	density, kg/m^3
ρ_ref	reference density, kg/m^3
σ_k	Prandtl number for the turbulent kinetic energy
σ_t	turbulent Prandtl number
σ_ε	Prandtl number for the turbulent kinetic energy dissipation rate

Subscripts

r	radial direction
z	axial direction

been proposed [2,3]. In the window configuration, the proton beam enters the target region through a thin solid barrier (window), which isolates the beam transport pipe and the liquid target. Various methods of circulating the liquid metal have been proposed consisting of pump driven, buoyancy driven and gas driven systems.

Typical buoyancy and gas-driven window modules are shown in Fig. 1. In the buoyancy driven module (Fig. 1a), flow of liquid metal of spallation target is induced by buoyancy force. A large value for volumetric expansion coefficient of LBE helps in this regard. The heat deposition by the proton beam raises the fluid temperature in the hot leg while the cold leg temperature is maintained through the secondary coolant flow in heat exchanger. The higher the temperature difference, greater will be the fluid flow. However, due to corrosion there will be an upper limit to the temperature difference (~150 °C) that has to be maintained [4]. In the gas-driven system (Fig. 1b), the effects of natural circulation are reinforced by way of mixing a gas to create two-phase flow in the riser leg, which increases available pressure head to drive the liquid metal flow. Bellucci et al. [5] has summarized the advantages of each configuration. However the spallation region of both these configurations and also that of pump driven system is the most critical in the design of the target module, and requires detailed fluid dynamic calculations to arrive at appropriate optimum dimensions. As can be seen in the window target module, high-density liquid metal spallation target and proton beam pipe, under vacuum environment, are separated by solid window barrier through which proton beam passes to interact with the target and deposit a bulk of the beam energy as heat. For a typical window material and geometry, the proton beam deposits tens of kW of heat in the window for few mA of beam current (~4 kW/mA current for 1 GeV beam [6,7]) and this deposition increases if the energy of the beam is lower [8]. Successful removal of heat deposited in the window by the circulating target is one of the critical thermal-fluid dynamic issues involved in target design.

The window barrier is a delicate component of the target system and has limited life, being exposed to the combined effects of high intensity proton and neutron irradiation, liquid metal corrosion and high thermal stresses induced due to the heat deposition by the proton beam. It is estimated that maximum proton current density the window can withstand is ~50 μA/cm^2 [5]. The velocity and temperature distribution in the spallation region crucially decide the capability of flow to remove the spallation heat. The problem is further compounded due to the requirement of relatively low velocities (to reduce corrosion and erosion) and availability of low-pressure heads (for buoyancy system due to limitation on temperature difference between riser and downcomer) for liquid metal flow. Detailed experiments have to be carried out to arrive at the optimum flow configuration that avoids flow stagnation and recirculation in the spallation region. In addition, the window being a key and probably the most fragile component in the whole system needs to be appropriately designed to withstand the thermal load. In view of this, an experimental LBE (lead 45%–bismuth 55%) [7] loop is being set up to study both thermal-hydraulic and material issues. A schematic of the proposed loop is shown in Fig. 2. The major components of the experimental loop consists of target module simula-

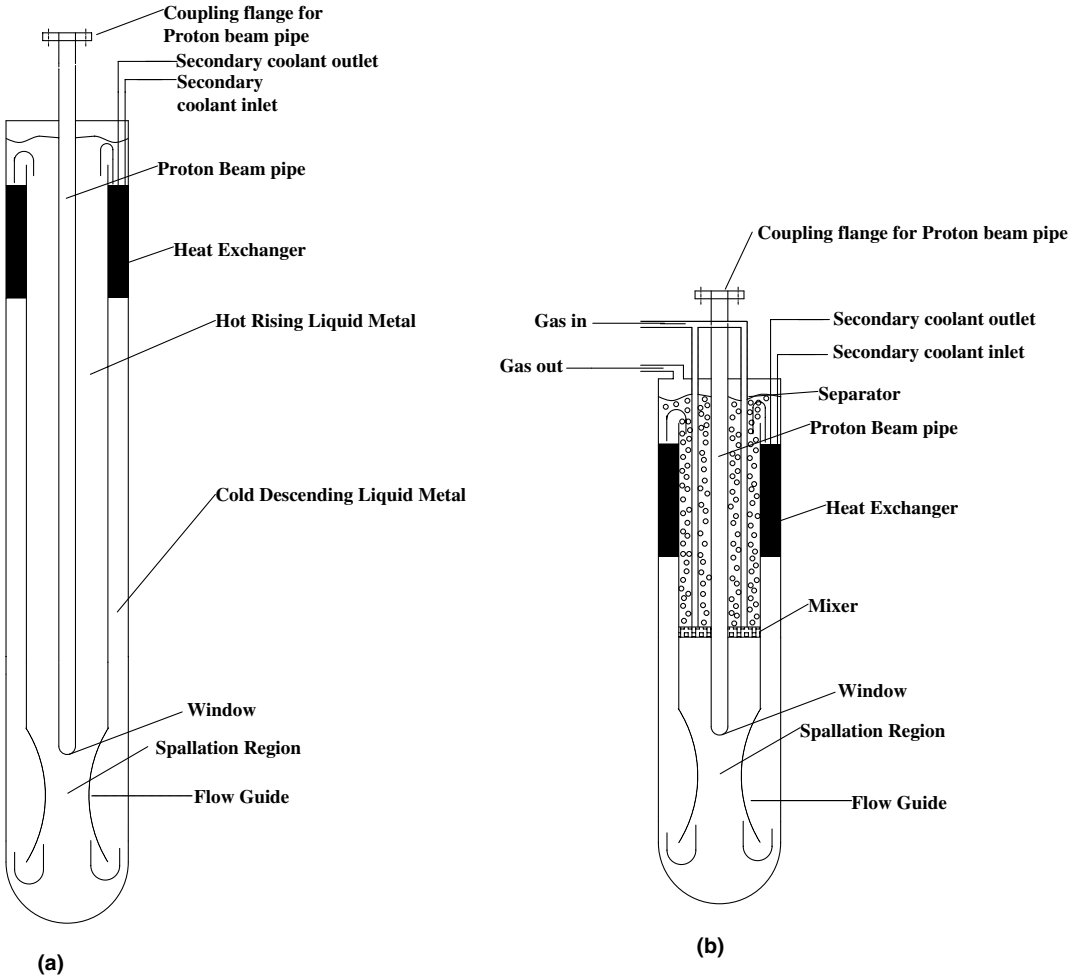

Fig. 1. Buoyancy and gas driven window target module.

tion region, separator, mechanical pump, heat exchanger, plasma torch and dump tank for LBE storage [7]. The mass flow rate (maximum of 120 kg/s) and the geometry of the loop will be 1:1 scale of the actual target (corresponding to a target of ~mA of beam current) and operating at 220 °C. The mechanical pump provides the required flow rate. The heat exchanger removes the heat deposited in the window. This facility is currently under design stage. A plasma torch has been developed to simulate window thermal loading [9]. In this paper, detailed thermal-hydraulic numerical analysis that has been carried out near the window region for different window materials, geometry, flow rates and heat loads for the window are presented.

The basic difference between the reactor target module and the experimental target module is the nature of the heat source. In the actual ADS, proton beam deposits volumetric heat in the window, and in the present simulation, the heat is supplied to the window from the inner surface of the window. Thus, the temperature distribution in the window will not be same as that of actual window. However, intense heating of the window with typical thermal loads as that of proton beam can be simulated. The plasma torch was designed in such a way that it is possible to vary the total heat deposition (up to 60 kW) as well as heat flux distribution (few kW/cm^2). Further, in the case of actual target, in addition to window heating, large volumetric heating in the flowing target takes place, which is not being simulated in the proposed experiments. The required plasma torch for the simulation studies has been presented with particular emphasis on flow and temperature distribution in and around the window.

2. Numerical solution

Various hemispherical window geometries having both uniform and variable window thickness (with minimum thickness at the centre) have been analyzed. The computational domain is shown in Fig. 3a. The liquid metal enters the flow guide from the bottom and flows upwards. From the exit of the flow guide, it flows in to the annular riser pipe after extracting the heat from window. Many materials have been proposed for window [10]. Analysis is carried out for different materials of construction to arrive at the optimum thermal load the window can take. The main purpose of the CFD analysis is, (1) to determine the thermal load the window experiences for the different materials, (2) to find out the temperature distribution in the window for the purpose

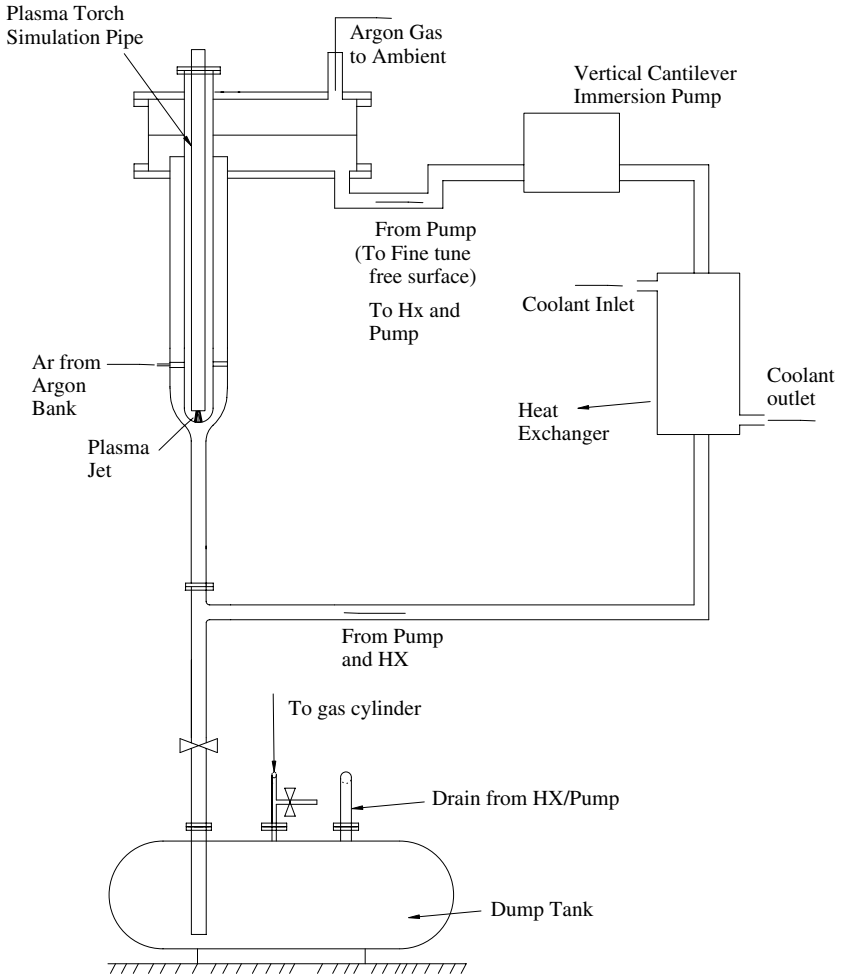

Fig. 2. The schematic of the proposed experimental facility with window target module.

of mechanical design, (3) to arrive at optimum geometry so that re-circulation or stagnation zones in the flow are not located in the heating zone or are minimized.

2.1. Governing equations

The governing equations are simplified by following assumptions: (i) geometry is limited to two dimensions, with the computational model having z-axis symmetry, (ii) neglecting swirl, flow is assumed two dimensional, and (iii) flow is assumed incompressible. For the buoyancy effect which is attributed to density, Boussinesq approximation is applied [11]. For the two flow rates considered here (40 kg/s and 120 kg/s) the corresponding Reynolds numbers are 1.6×10^5 and 4.8×10^5, which clearly denote that the flow is in the turbulent regime. The closure problem of the turbulent modeling is solved using k–ε model with appropriate wall functions [11]. The surface heat supplied by plasma jet, flows from the inner surface of the window to the outer surface by conduction, from where the heat is to be carried away by the flowing LBE by mixed convection. LBE has a very low Prandtl number (~0.02) and hence temperature gradients in the solid window and the fluid are comparable. Therefore, in order to arrive at the proper window temperature profile, a conjugate heat transfer problem has been solved. The conservation of mass, momentum, energy, and k–ε model equations for the fluid and heat conduction for the window can be written as [11–13]

Continuity equation:

$$\frac{1}{r}\frac{\partial(\rho r u_r)}{\partial r}+\frac{\partial(\rho u_z)}{\partial z}=0, \tag{1}$$

where, u_z, u_r are the components of velocity vector in the z and r directions, ρ is the density of the liquid metal.

Radial momentum equation:

$$\frac{\partial\rho u_r}{\partial t}+\frac{1}{r}\frac{\partial(\rho r u_r u_r)}{\partial r}+\frac{\partial(\rho u_z u_r)}{\partial z} = -\frac{\partial p}{\partial r}+\frac{1}{r}\frac{\partial}{\partial r}\left(\mu_e r\frac{\partial u_r}{\partial r}\right)+\frac{\partial}{\partial z}\left(\mu_e\frac{\partial u_r}{\partial z}\right)-\mu_e\frac{u_r}{r^2}. \tag{2}$$

Axial momentum equation:

$$\frac{\partial\rho u_z}{\partial t}+\frac{1}{r}\frac{\partial(\rho r u_r u_z)}{\partial r}+\frac{\partial(\rho u_z u_z)}{\partial z} = -\frac{\partial p}{\partial z}+\frac{1}{r}\frac{\partial}{\partial r}\left(\mu_e r\frac{\partial u_z}{\partial r}\right)+\frac{\partial}{\partial z}\left(\mu_e\frac{\partial u_z}{\partial z}\right)+(\rho_{ref}-\rho)g_z, \tag{3}$$

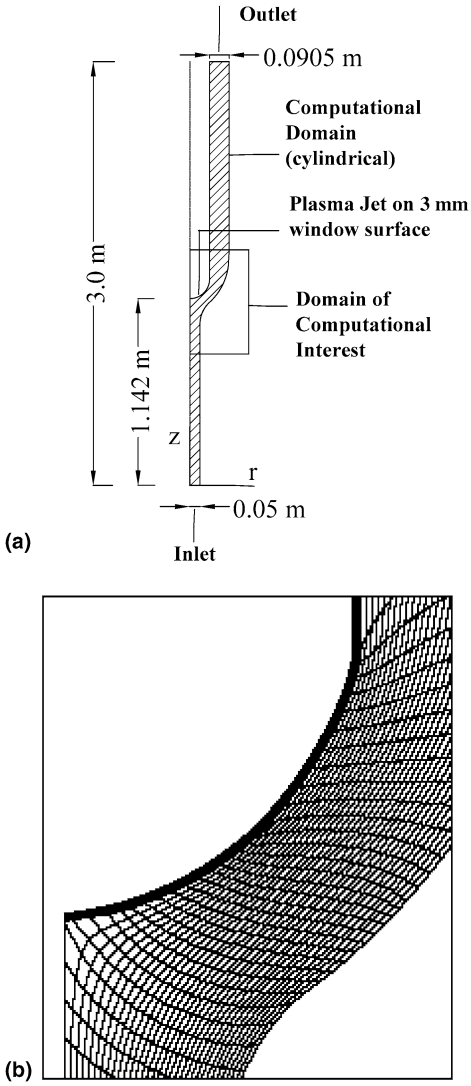

Fig. 3. (a) The schematic of the computational domain and (b) grid near the window region.

where, p is pressure, μ_e is effective viscosity, ρ_{ref} is reference density corresponding to inlet density of the liquid metal and g_z is the acceleration due to gravity. Here, u_z, u_r, ρ, p are time averaged values.

Energy equation:

$$\frac{\partial \rho C_p T}{\partial t}+\frac{1}{r}\frac{\partial\left(\rho C_p r u_r T\right)}{\partial r}+\frac{\partial\left(\rho C_p u_z T\right)}{\partial z} =\frac{1}{r}\frac{\partial}{\partial r}\left(r\Gamma_k\frac{\partial T}{\partial r}\right)+\frac{\partial}{\partial z}\left(\Gamma_k\frac{\partial T}{\partial z}\right), \tag{4}$$

where, C_p is specific heat at constant pressure and T is time-averaged temperature.

The effective viscosity μ_e and effective conductivity Γ_k are given by

$$\mu_e=\mu_m+\mu_t, \tag{5}$$

$$\Gamma_k=\left(k_m+\frac{\mu_t C_p}{\sigma_t}\right). \tag{6}$$

The turbulent viscosity is given by

$$\mu_t=C_\mu\rho\frac{k^2}{\varepsilon}, \tag{7}$$

where, μ_m is molecular viscosity, C_μ is the turbulent model constant, k_m is molecular thermal conductivity. Note that viscous heating is neglected. The turbulent kinetic energy (k) and turbulent kinetic energy dissipation rate (ε) are given by the following equations:

Turbulent kinetic energy equation:

$$\frac{\partial \rho k}{\partial t}+\frac{1}{r}\frac{\partial(\rho r u_r k)}{\partial r}+\frac{\partial(\rho u_z k)}{\partial z} =\frac{1}{r}\frac{\partial}{\partial r}\left(r\frac{\mu_t}{\sigma_k}\frac{\partial k}{\partial r}\right)+\frac{\partial}{\partial z}\left(\frac{\mu_t}{\sigma_k}\frac{\partial k}{\partial z}\right)+S_k+\frac{\beta\mu_t}{\sigma_T}\left(g_z\frac{\partial T}{\partial z}\right), \tag{8}$$

where, μ_t is turbulent viscosity, σ_k is Prandtl number for the turbulent kinetic energy. The last term in Eq. (8) is used to model the effect of buoyancy. S_k the net turbulence kinetic energy source term is given by

$$S_k=G-\rho\varepsilon, \tag{9}$$

$$G=\mu_t\left\{2\left[\left(\frac{\partial u_r}{\partial r}\right)^2+\left(\frac{\partial u_z}{\partial z}\right)^2+\left(\frac{u_r}{r}\right)^2\right]+\left(\frac{\partial u_z}{\partial r}+\frac{\partial u_r}{\partial z}\right)^2\right\}, \tag{10}$$

where, G is turbulent kinetic energy source term, generated due to mean velocity gradient.

Dissipation rate equation:

$$\frac{\partial \rho\varepsilon}{\partial t}+\frac{1}{r}\frac{\partial(\rho r u_r \varepsilon)}{\partial r}+\frac{\partial(\rho u_z \varepsilon)}{\partial z} =\frac{1}{r}\frac{\partial}{\partial r}\left(r\frac{\mu_t}{\sigma_\varepsilon}\frac{\partial \varepsilon}{\partial r}\right)+\frac{\partial}{\partial z}\left(\frac{\mu_t}{\sigma_\varepsilon}\frac{\partial \varepsilon}{\partial z}\right)+S_\varepsilon+\frac{C_{1\varepsilon}\varepsilon}{k}B, \tag{11}$$

where,

$$S_\varepsilon=\frac{\varepsilon}{k}(C_{1\varepsilon}G-C_{2\varepsilon}\rho\varepsilon), \tag{12}$$

$$B=\frac{\beta\mu_t}{\sigma_t}\left(g_z\frac{\partial T}{\partial z}\right), \tag{13}$$

where, σ_ε is Prandtl number for the turbulent kinetic energy dissipation rate, β is coefficient of thermal expansion used in buoyancy terms. The last term in Eq. (11) is used to model the effect of buoyancy. The following values have been taken for the various coefficients in the turbulent model [11]: $C_{1\varepsilon}=1.44$, $C_{2\varepsilon}=1.92$, $C_\mu=0.09$, $\sigma_k=1.0$, $\sigma_\varepsilon=1.3$, $\sigma_T=0.9$, $\beta=1.28\times10^{-4}\,K^{-1}$. The LBE properties are taken from Buono [14].

2.2. Boundary conditions

Velocity components are specified at the inlets along with temperature (220 °C), for two flow rates (40 kg/s and

120 kg/s). Outlet pressure is taken as 2.0×10^5 N/m^2. No slip boundary condition has been implemented for the walls of riser pipe and the proton beam pipe including window. Symmetry condition has been invoked along the axis of the proton beam pipe and analysis is carried out for one half of the physical domain to save computational time. The window and the proton beam simulator pipe wall were assumed thermally conducting and the outer riser wall adiabatic.

In conjugate heat transfer problems, the continuity of temperature and heat flux at the liquid metal and the window interface is expressed by equating the heat flux of the liquid metal with the heat flux of the window wall and by equating the temperature of the liquid metal with the temperature of the wall, at the interface. Wall function approach given by Launder and Spalding [11] for low Prandtl number fluids has been implemented for the turbulent flow analysis.

2.3. Numerical scheme

The numerical investigations were accomplished using a segregated finite element method based on streamline upwind Petro–Galerkin technique (SUPG) developed by Brooks and Hughes [15]. Time-dependant transport equations of momentum, energy, turbulent kinetic energy and energy dissipation rate are solved following the Eulerian velocity correction approach based on SIMPLE algorithm [16]. The incomplete Choleski conjugate gradient method has been used for solving pressure equation [17]. The Galerkin method is used to solve the conduction equation in the solid window. In order to validate the SUPG scheme, two model problems were tested, namely, the backward-facing step and the buoyancy-driven cavity problems using 2-D orthogonal grids. With a parabolic velocity profile at the inlet, downstream boundary at $x = 20$ h, and a 21×101 grid, the reattachment lengths obtained for laminar flow in a backward-facing step for different Reynolds number are compared with the experimental results due to Armaly et al. [18] in Fig. 4. As seen in Table 1, results are obtained for a buoyancy-driven cavity for Prandtl number 0.7 (air) for different Raleigh numbers with a 77×77 grid are in excellent agreement with the solution of de Vahl Davis et al. [19].

2.4. Grid

Structured grids have been generated using partial differential equation technique (Laplace equation). Higher grid refinement was ensured for the fluid zone near the window (5×50), which is the region of interest. The grids thus generated in the r–z domain of interest are shown in Fig. 3b.

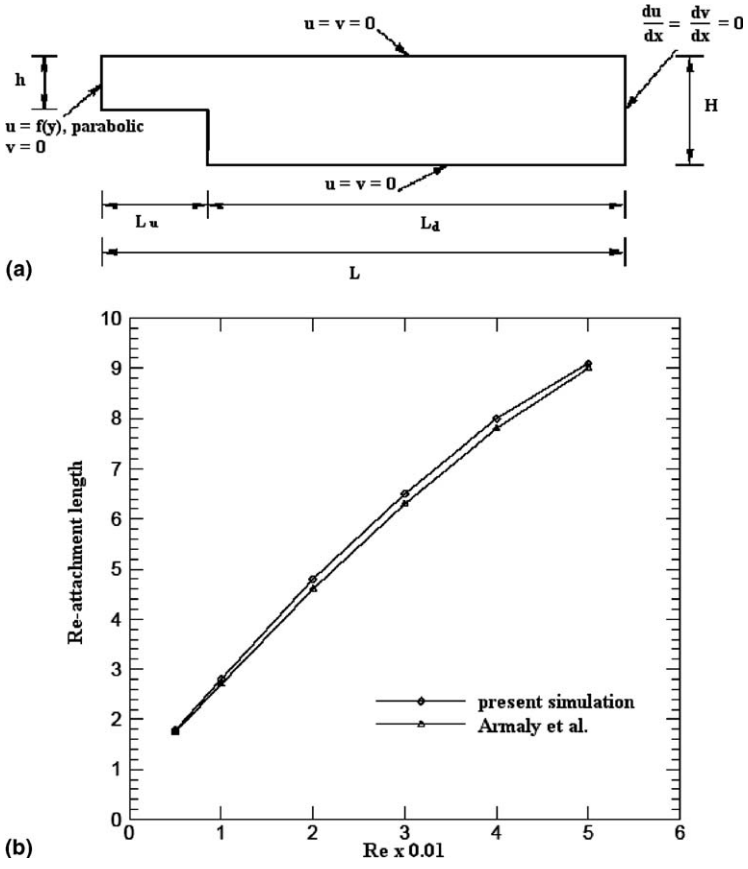

Fig. 4. (a) 2-D backward-facing step problem and (b) validation of reattachment length with Reynolds number.

Table 1
Comparison of different parameters in a buoyancy-driven flow in a lid for different Raleigh numbers

	De Vahl Davis	Present computation	Error (%)
(a) Ra = 10^3			
u_{max}	3.649	3.630	0.52
y	0.813	0.809	
v_{max}	3.697	3.732	0.95
x	0.178	0.178	
Nu_{max}	1.505	1.514	−0.60
Y	0.092	0.094	
Nu_{min}	0.692	0.706	−2.02
x	1.0	1.0	
(b) Ra = 10^4			
u_{max}	16.178	16.117	0.37
y	0.823	0.829	
v_{max}	19.617	19.54	0.39
x	0.119	0.118	
Nu_{max}	3.528	3.445	2.35
Y	0.143	0.145	
Nu_{min}	0.586	0.581	0.85
x	1.0	1.0	
(c) Ra = 10^5			
u_{max}	34.73	34.739	−0.03
y	0.855	0.860	
v_{max}	68.59	68.215	0.55
x	0.066	0.066	
Nu_{max}	7.717	7.723	−0.08
Y	0.081	0.085	
Nu_{min}	0.729	0.738	−1.23
x	1.0	1.0	

3. Results and analysis

3.1. Spatial grid independence test

The plots shown in Fig. 5 obtained for three different meshes; show a maximum deviation of less than 5% while predicting Nusselt number for grid size of 33×109. In the present analysis, computation has been performed with a 33×109 mesh for the fluid and a 5×48 mesh for the window.

3.2. Thermal-hydraulic analysis of window target of the simulation facility

In this analysis, studies have been carried out for three different window materials namely SS-321, T-91, W-26%Re. The composition of SS-321, T-91, and W-26%Re are summarized in Table 2. Analysis was carried out for different window thermal loads, various window thicknesses (2 mm and 3 mm); various beam profiles (narrow, i.e., focused and spread, i.e., diffused plasma heat flux profiles), also with variable thickness of window (1.5 mm at the centre and 3 mm at the edge). From proton heat deposition point of view thin window is better as compared to higher thickness. However, from the requirement of structural strength, higher thickness is preferable. An optimized design will be smaller thickness at the centre of the window (where maximum beam current is expected) and progressively increasing thickness towards the edges. All these analyses were carried out for two flow rates (40 kg/s and 120 kg/s) and keeping the inlet flow temperature at 493 K. In addition, for a typical flow and thermal load, the effect of geometric shape on the flow behavior has been analyzed. In view of this, analysis has been carried out for all these configurations. The actual window geometry will have to satisfy all these requirements including the damage caused by radiation. The actual thermal load the window can take will be further decided by mechanical design of the window pipe and window (welding of the window with pipe, where and how the window pipe will be anchored, etc.). Here we have presented suitable heat loads which window can withstand, from the thermal-hydraulics point of view.

The velocity distribution, for a typical heat load of 17 kW for a T91 window with thickness varying from 1.5 mm in center to 3 mm at the edges and flow rate of 120 kg/s is presented in Fig. 6. It can be seen that a re-circulating zone is present at the entrance of the annular flow region. Since this is located outside the window region, it has relatively no bearing on the window cooling but may lead to higher-pressure drop in the loop. In Fig. 7, the turbulent kinetic energy has been plotted. The maximum value obtained was 0.1633 m^2/s^2. This is in the region near the window, contributing towards cooling of window. The fluid with high velocity experiences sudden deceleration, near the window, due to which the region has high mean velocity gradient. Consequently, the production of turbulent kinetic energy is high, which gives rise to high turbulent kinetic energy value in this region. The turbulent energy dissipation rate is maximum near the window region and has a value of 14.46 m^2/s^3 (see Fig. 8). Fig. 9 gives the corresponding temperature distribution in the fluid and window. The temperature distribution on the two surfaces of the window along with heat flux distribution is presented in Fig. 10. The given heat flux is more or less uniformly distributed on the window with maximum flux of 2.2 MW/m^2. We see maximum window temperature both on the plasma torch side as well as fluid side, is away from the centre. The same trend was observed for all the cases. This is primarily because of the absence of any eddy formation near the centre of the window as expected [20]. The cold liquid metal after extracting the heat near the centre gets heated up before extracting the heat away from the centre. This increases the temperature on the window surface at a location shifted from centre. Summary of the temperatures on the window for various geometries, materials and flow conditions are presented in Tables 3–6. The studies have been carried out for 40 kg/s and 120 kg/s which corresponding to 0.5 m/s and 1.5 m/s average velocity at the entrance. The heat flux profile is assumed uniform up to a radius of 4 cm and falling sharply beyond up to 7 cm (see Fig. 10). The heat loads for each of the configuration are determined such that the maximum temperature on the window is within the operable range of the material

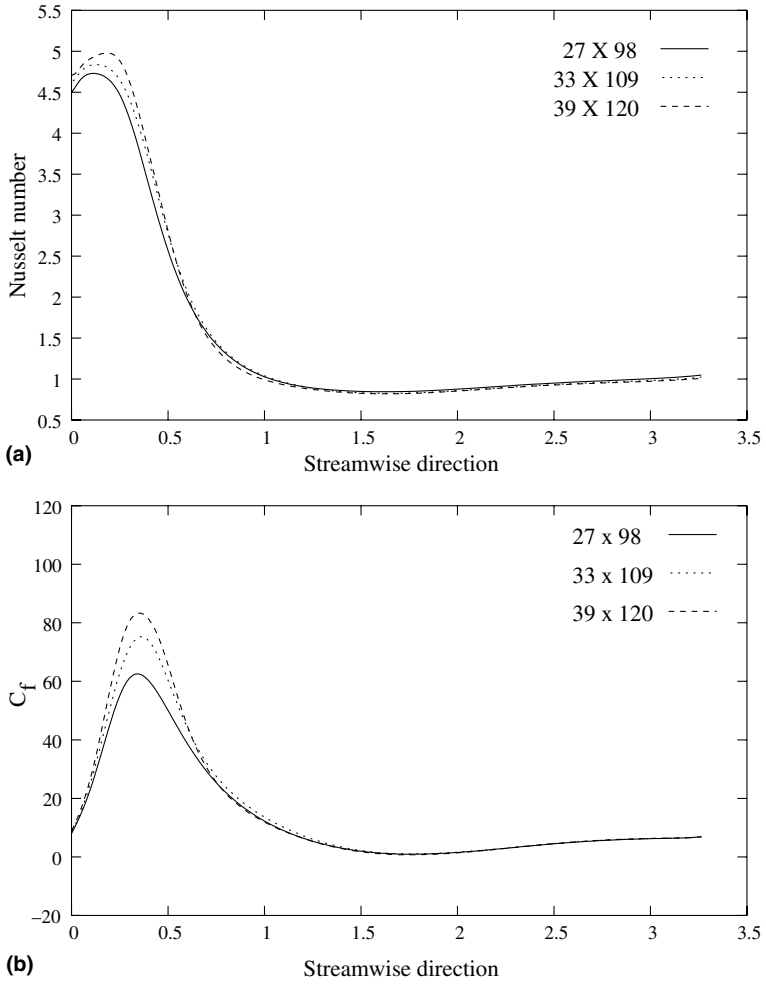

Fig. 5. Grid independence test: (a) Nusselt number and (b) $C_f \times Re$ distribution along the streamwise direction for three different grids.

Table 2
Composition and operating temperature of various window materials for CHT analysis

	Material type	Composition of window material in weight percent	Proposed operating temperature[a] (°C)
1	SS321	18Cr + 10Ni + 0.002Ti + 2.09Mo + 1.61Mn + 0.022C + 0.43Si + 0.024P + 0.019S + 0.18Cu + (Balance)Fe	600
2	T91	(0.08–0.12)C + (0.3–0.6)Mn + 0.02P + 0.01S + (0.2–0.5)Si + (8–9.5)Cr + (0.85–1.05)Mo+0.4Ni + (0.18–0.25)V + (0.03–0.07)N + (0.06–0.1)Nb + 0.04Al + (balance)Fe	600–800
3	W-26%Re	26Re + (balance)W	1000

[a] The thermal stress analysis will also contribute to the operating temperature of window. The operating temperature is listed as per thermal analysis only.

(see Table 2). For a 2 mm uniformly thick SS321 window, for a heat load of 17 kW, the maximum temperature in the window is around 800 K for the flow rate of 40 kg/s and due to better cooling, the temperature is 770 K for 120 kg/s flow rate (see Table 3). When the thickness of the window is 3 mm, the maximum temperature has increased to 900 K and 878 K (without much change in the temperature distribution on the window surface which is in contact with liquid metal), respectively, for different flow rates as expected due to higher window thickness. For the case of T91 window (Table 3, Figs. 11 and 12) due to higher thermal conductivity, it is possible to deposit around 30 kW of heat, keeping the maximum window temperature range similar to that of SS321. In the case of W-26%Re window, it is even possible to load up to 65 kW of heat. This is mainly due to higher operating temperature and thermal conductivity of the material. Even though this analysis gives typical optimum loads the window can take, the actual load is further decided by the thermal stress analysis. Preliminary stress analysis was carried out with axis-

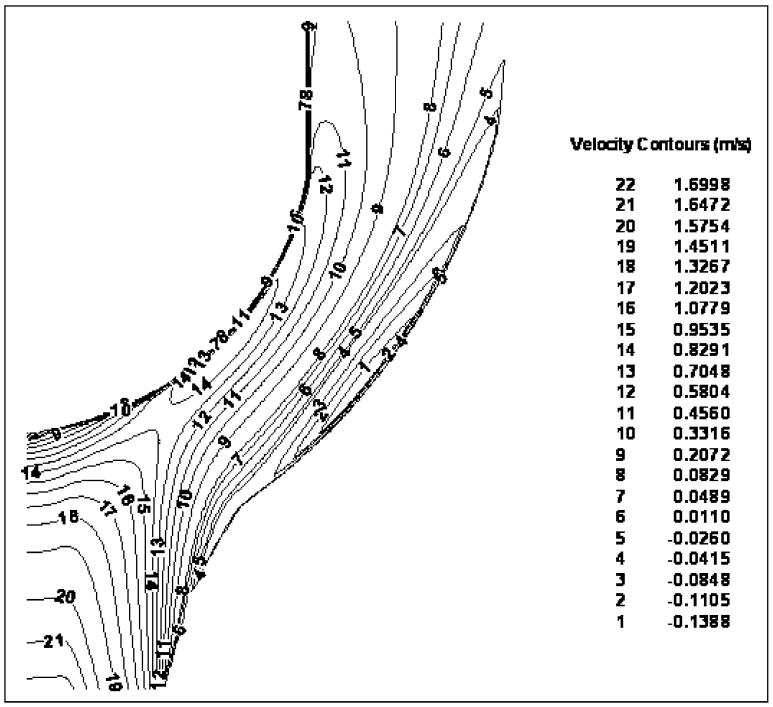

Fig. 6. Window target configuration velocity contours (mass flow rate = 120 kg/s, plasma power = 17.0 kW, inlet temperature 493 K, T91 window with varying thickness from 3 mm on sides to 1.5 mm in the center of window).

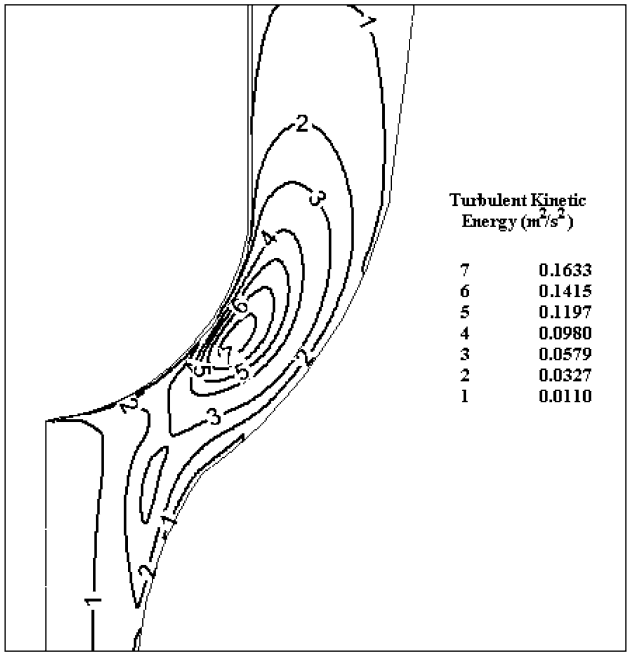

Fig. 7. Window target configuration turbulent kinetic energy contours (mass flow rate = 120 kg/s, plasma power = 17.0 kW, inlet temperature 493 K, T91 window with varying thickness from 3 mm on sides to 1.5 mm in the center of window).

symmetric elements applying loads available from numerical flow solution. The Von Mises stresses were found to be less than 150 MPa for 22 kW of heat load in the T91 window of 3 mm uniform thickness. This indicates that thermal stresses are comfortably below the operational range (UTS of T91 is ~800 MPa [21]). The results corresponding to variable thickness of the window (1.5 mm at the centre and 3 mm at the edges with outer hemispherical shape for window) are summarized in Table 4 (Fig. 10). The analysis was carried out for a typical heat loads.

In order to study the effect of heat flux distribution for the same total heat deposition, a typical analysis has been carried out for two different heat flux distributions corresponding to 20 kW for T91 window with variable thickness. The results are plotted in Fig. 13. For the case where the heat flux is 1.4 MW/m^2 (maximum), the maximum window temperature is around 778 K. For the second case with a maximum heat flux of around 1 MW/m^2, the maximum temperature reduced to around 619 K. We can further see that the temperature dip at the centre of the window remained more or less same for both the cases (see Table 5).

3.3. Effect of geometry near the window region

One of the important flow regions is near the window. Transition of the flow from pipe flow to annular flow takes place near the window. The flow in this region is expected to affect the window cooling capability of the liquid metal for a typical mass flow rate and also cause additional pressure losses if there are large recirculation regions. Preliminary analysis has been carried out to see the sensitivity of the transition region on the window cooling. In addition to the original geometry (C1), three more configurations (C2, C3,

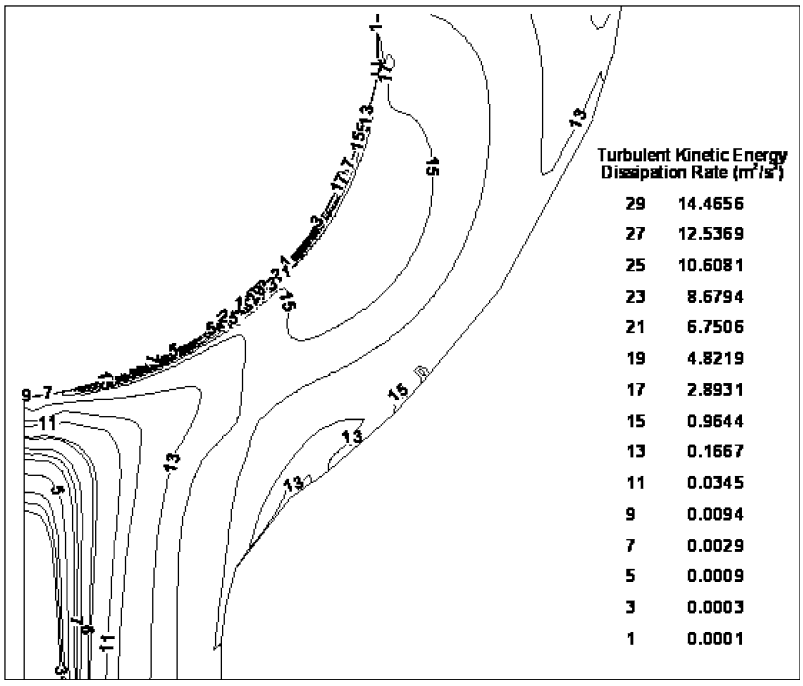

Fig. 8. Window target configuration turbulent kinetic energy dissipation rate contours (mass flow rate = 120 kg/s, plasma power = 17.0 kW, inlet temperature 493 K, T91 window with varying thickness from 3 mm on sides to 1.5 mm in the center of window).

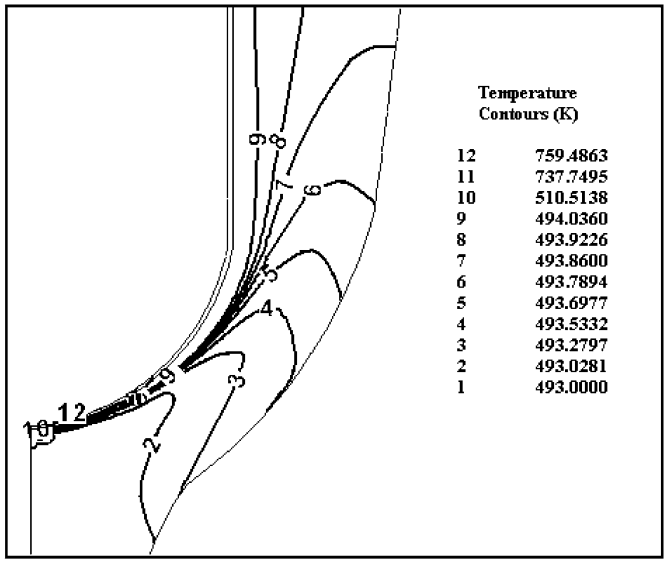

Fig. 9. Window temperature contour (mass flow rate = 120 kg/s, plasma power = 17.0 kW, inlet temperature 493 K, T91 window with varying thickness from 3 mm on sides to 1.5 mm in the center of window).

and C4) have been studied (see Table 6). In all these cases, the analysis has been carried out for 120 kg/s mass flow rate, variable window width (3 mm at the edges and 1.5 mm at the centre) of T91, with inlet temperature of 493 K. The thermal load on the window is 22 kW. The window geometry, pipe diameter below the window, annular riser pipe diameters has been taken same for all these cases. The velocity contours for various configurations has been shown in Figs. 14–17. Configuration C1 is the geometry studied for all the previous cases. Fig. 14 gives the velocity contours and we see that, there is large low velocity region at the outer transition region. Another analysis has been carried out keeping the window same as that of C1 but outer transition region has been reduced as shown in Fig. 15. This essentially reduces the recirculation region and is shifted upwards. Also there is increased in velocity of the fluid near the window region. We see that the maximum window temperature was reduced to 569 K. This seems to be better configuration than the case C1. In configuration C3, window shape has been made oblique and also outer flow regime has been reduced. There is a drop in the maximum window temperature, primarily due to larger window being exposed to plasma heat, thus reducing the heat flux density. In addition we see that the low velocity as well as recirculation zone has relatively reduced as seen in Fig. 16. Based on this we have kept the window configuration same as that of C3 but the outer flow region has been reduced further (Fig. 17). The maximum temperature is now 711 K. The reason may be due to decrease in the liquid velocity near the window region. This further confirms necessity of optimizing the geometry of the transition region for optimum window cooling.

4. Plasma torch for window heat simulation

The ideal ADS heat flux simulator should deliver the type of heat flux (magnitude and profile) required to simulate the window heat load that will be produced by the proton beam. The actual heat deposited will depend on beam energy, current, beam profile and window material.

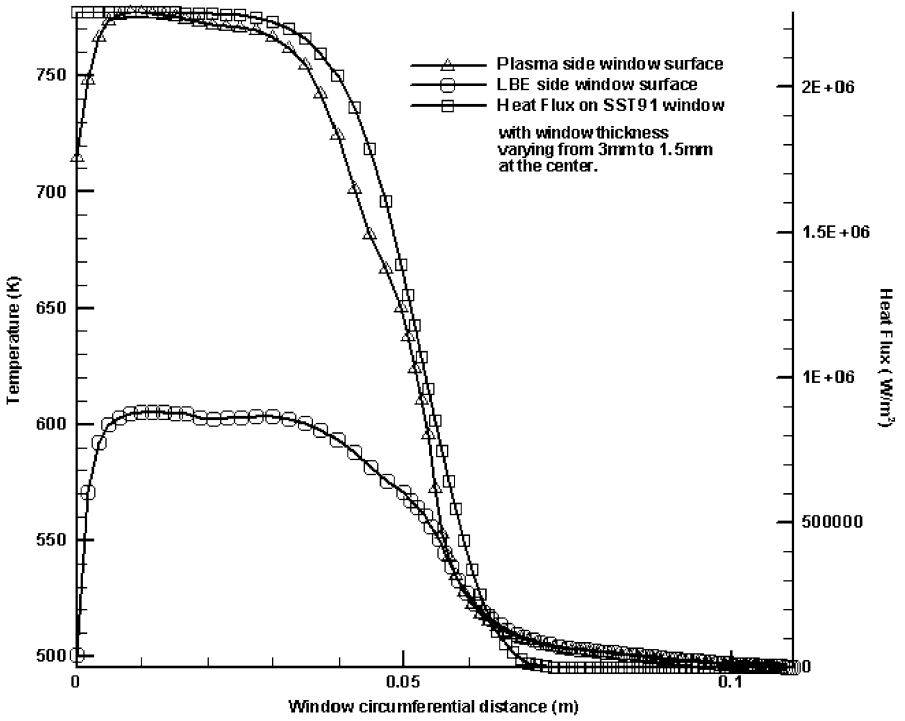

Fig. 10. Window surface temperature distributions on plasma and LBE side (mass flow rate = 120 kg/s, plasma power = 17.0 kW, inlet temperature 493 K, T91 window with varying thickness from 3 mm on sides to 1.5 mm in the center of window).

Table 3
The results of CFD simulation for SS321, SST91, W-26%Re target window with different thickness and optimized plasma power applied on window, respectively

Sr. No.	Window material	Thickness of window (mm)	Average inlet velocity (m/s)	Mass flow rate (kg/s)	Thermal load (kW)	Window maximum temperature (K)	Inlet temperature (K)	Temperature of window surface in contact with LBE (K)	
								T_{max}	T_{min}
1	SS321	2.0	0.5	40	17.2	802	493	610	496
			1.5	120	17.2	770	493	574	493
		3.0	0.5	40	17.8	900	493	600	497
			1.5	120	17.8	878	493	573	493
2	T91	2.0	0.5	40	30.0	873	493	685	500
			1.5	120	30.0	822	493	630	493
		3.0	0.5	40	19.5	872	493	640	500
			1.5	120	19.5	827	493	593	493
3	W-26%Re	2.0	0.5	40	65.5	1097	493	910	510
			1.5	120	65.5	985	493	792	495
		3.0	0.5	40	65.6	1215	493	902	510
			1.5	120	65.6	1108	493	516	493

However, typical heat loads will be around tens of kilowatts. In this analysis, a typical uniform heat flux profile is assumed. However the total heat deposited on the window will be typical of the proton beam (tens of kilowatts with few kW/cm^2). The plasma torch developed will provide these requirements.

Plasma torch is a thoriated tungsten tapered rod cathode, with a nozzle-shaped copper anode through which the hot plasma jet exits on to the window substrate. The plasma torch is capable of operating both in transferred and non-transferred arc modes. In transferred arc mode, the torch is capable of operating up to 120 kW (300 V, 400 A) at about 95% efficiency and is capable of sustaining an arc length of about 200 mm stand off (distance between torch and substrate). Out of this power ~50% will be deposited in the window (the rest is carried away by

Table 4
The results of CFD simulation for SS321, T91, W-26%Re target window with variable thickness and optimized plasma power applied on window, respectively

Sr. No.	Window material	Thickness of window at the center (mm)	Average inlet velocity (m/s)	Mass flow rate (kg/s)	Thermal load (kW)	Window maximum temperature (K)	Inlet temperature (K)	Temperature of window surface in contact with LBE (K)	
								T_{max}	T_{min}
1	S321	1.5	0.5	40	13	703	493	585	496
			1.5	120	13	689	493	566	495
2	T91	1.5	0.5	40	17	797	493	632	497
			1.5	120	17	777	493	604	495
3	W-26%Re	1.5	0.5	40	60	1059	493	910	508
			1.5	120	60	980	493	824	501

Table 5
The results for T91 window with variable plasma power beam applied on window, respectively

Sr. No.	Plasma heat flux profile	Average Inlet Velocity (m/s)	Mass flow rate (kg/s)	Thermal load (kW)	Window maximum temperature (K)	Inlet temperature (K)	Temperature of window surface in contact with LBE (K)	
							T_{max}	T_{min}
1	Wide	1.5	120	20	619	493	548	497
2	Narrow	1.5	120	20	778	493	566	495

Table 6
Effect of geometric configurations near the window region on T91 window temperature distribution

Sr. No.	Window configuration	Thickness of window at the center (mm)	Average Inlet Velocity (m/s)	Mass flow rate (kg/s)	Thermal load (kW)	Window maximum temperature (K)	Inlet temperature (K)	Temperature of window surface in contact with LBE (K)	
								T_{max}	T_{min}
1	C1	1.5	1.5	120	22.0	781	493	609	493
1	C2	1.5	1.5	120	22.0	569	493	456	293
2	C3	1.5	1.5	120	22.0	626	493	487	289
3	C4	1.5	1.5	120	22.0	711	493	599	494

cooling water and plasma gas). Thus the torch has the capability to provide a maximum of 60 kW of thermal load on the window. The gas flow rates vary from 5 LPM to 50 LPM depending on stability and voltage requirements. Argon or its mixture with nitrogen and hydrogen are used as the plasmogen gases. Since the torch has to go inside a long tube (see Fig. 2), easy replacement of the electrode modules is mandatory. Moreover, the body of the torch, the nozzle and cap should be protected from the heat as well as hot gases reflected from the window. Fig. 18 depicts the schematic of the plasma torch developed for this purpose. The torch is built around a nylon insulator of 100 mm diameter and 80 mm long and a SS spacer of 165 diameter and 30 mm long as shown in the diagram. A replaceable rod type cathode (2% Th – Tungsten) and a copper nozzle are housed inside the combined assembly of the insulator and the spacer. A large diameter copper cap is screwed to the spacer to protect the nozzle and the body of the torch from the reflected heat from the window. The complete assembly is again housed in a SS jacket and secured with screws, which is in turn welded to a 200 mm long 5″ NB-80-schedule SS pipe. The other end of the pipe is again welded to a 5″ NB SS flange. The cathode, anode, cap, jacket and the pipe are intensely water-cooled. All the water and gas connections are taken from inside the 5″ NB pipe. All the replaceable parts are provided with "O" rings to prevent water and gas leakages.

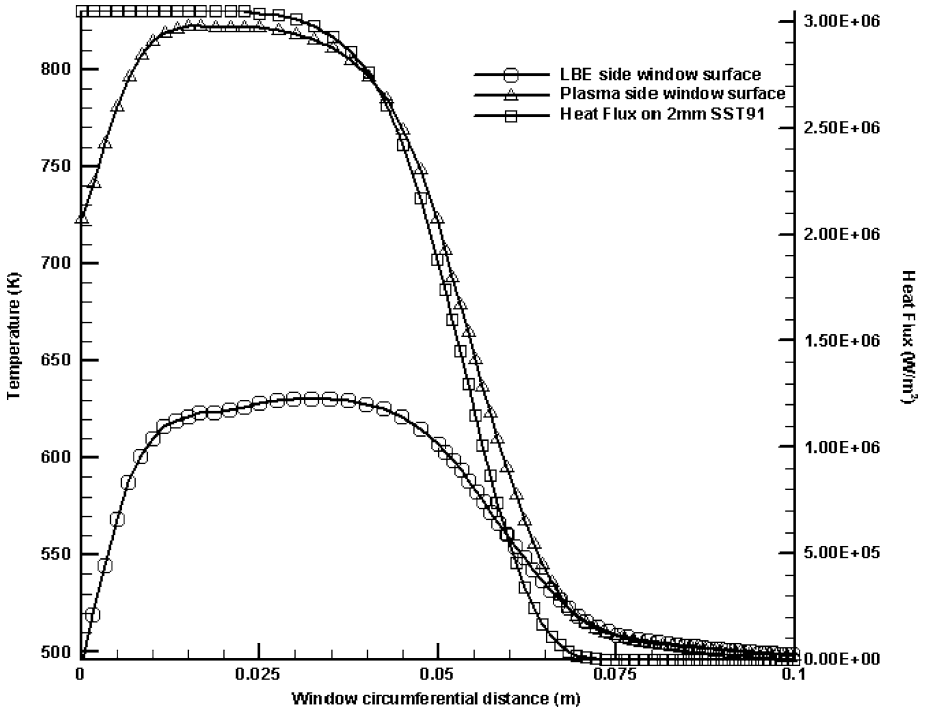

Fig. 11. Window surface temperature distribution on plasma and LBE side (mass flow rate = 120 kg/s, plasma power = 30.0 kW, inlet temperature 493 K, T91 window with uniform thickness of 2 mm throughout).

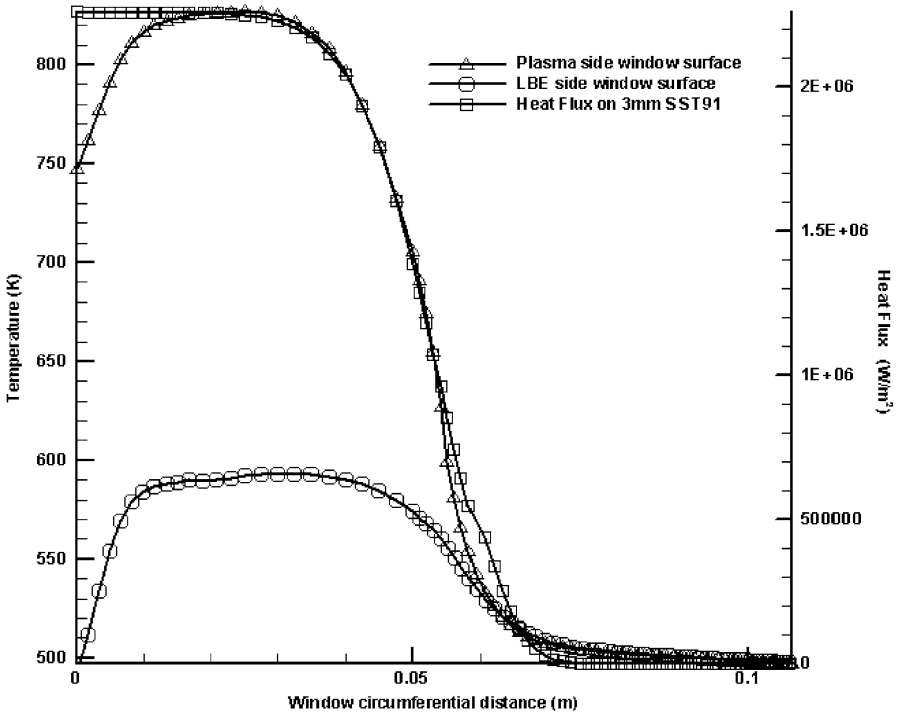

Fig. 12. Window surface temperature distribution on plasma and LBE side (mass flow rate = 120 kg/s, plasma power = 19.0 kW, inlet temperature 493 K, T91 window with uniform thickness of 3 mm throughout).

5. Testing the performance of the plasma torch in a water cooled window dish

The plasma torch is mounted coaxially inside an 8″ SS pipe (see Fig. 19). One end of the pipe fitted with a 250 mm radius dish end with a central 80 mm diameter copper window. The dish end, window and the pipe are intensely water-cooled. Two window sizes have been experimented upon, i.e., 50 mm and 80 mm diameter copper discs.

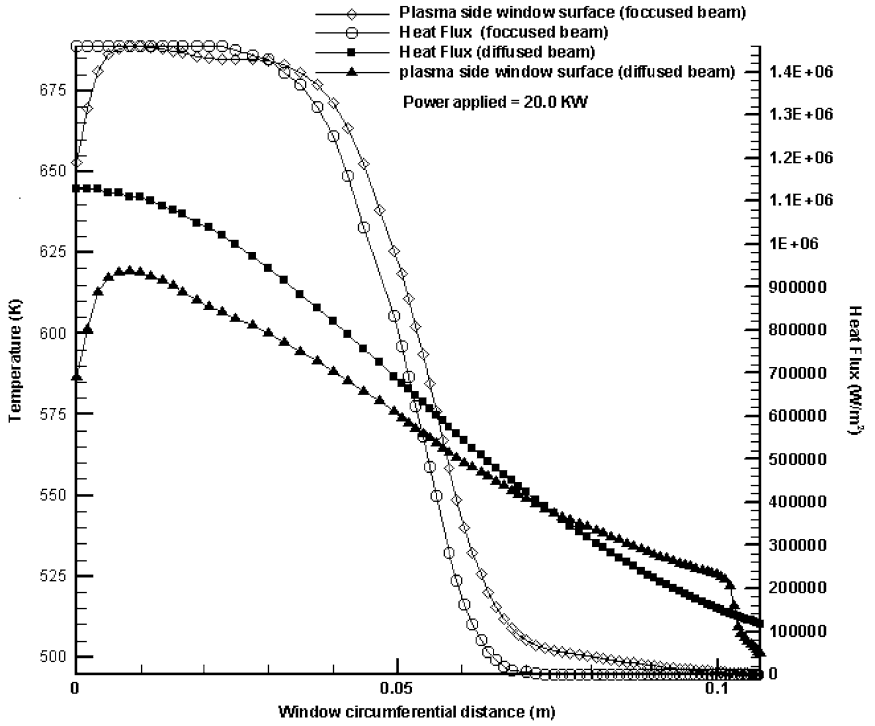

Fig. 13. The effect of plasma beam focusing on window surface temperature distributions on plasma side (mass flow rate = 120 kg/s, plasma power = 20.0 kW, inlet temperature 493 K, T91 window with varying thickness from 3 mm on sides to 1.5 mm in the center of window).

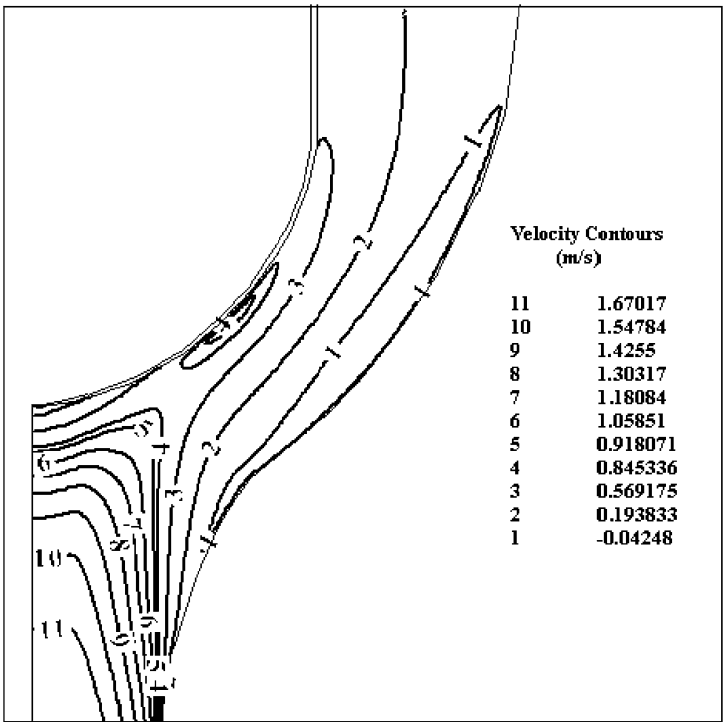

Fig. 14. Window target C1 velocity contour (mass flow rate = 120 kg/s, plasma power = 22.0 kW, inlet temperature 493 K, T91 window with varying thickness from 3 mm on sides to 1.5 mm in the center of window).

The plasma torch was ignited with a high frequency igniter and a pilot non-transferred arc jet is initially generated. The torch is lowered through a lead screw arrangement so that the distance between the torch and the window simulator is kept about 30–40 mm. The arc is now transferred on to this window simulator by applying a higher positive

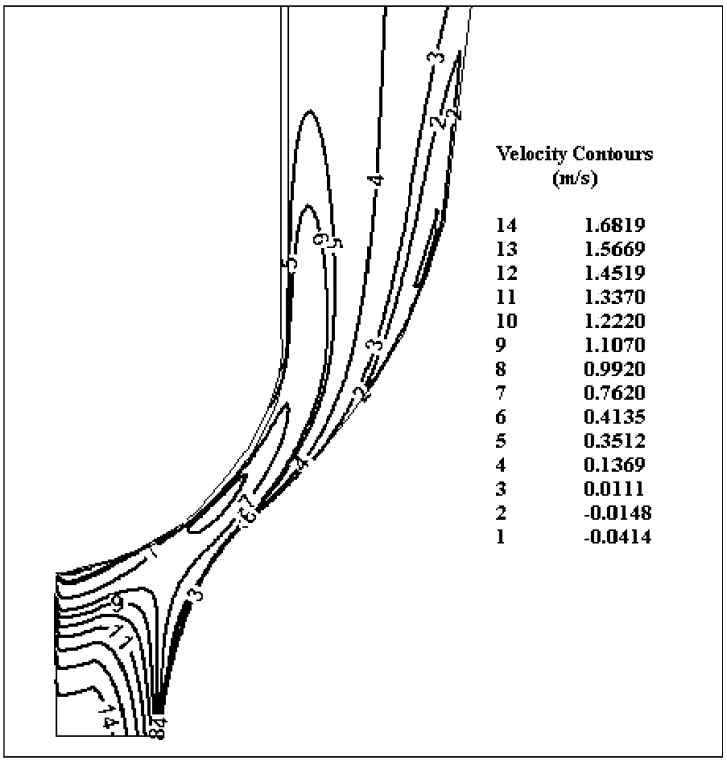

Fig. 15. Window target C2 velocity contours (mass flow rate = 120 kg/s, plasma power = 22.0 kW, inlet temperature 493 K, T91 window with varying thickness from 3 mm on sides to 1.5 mm in the center of window).

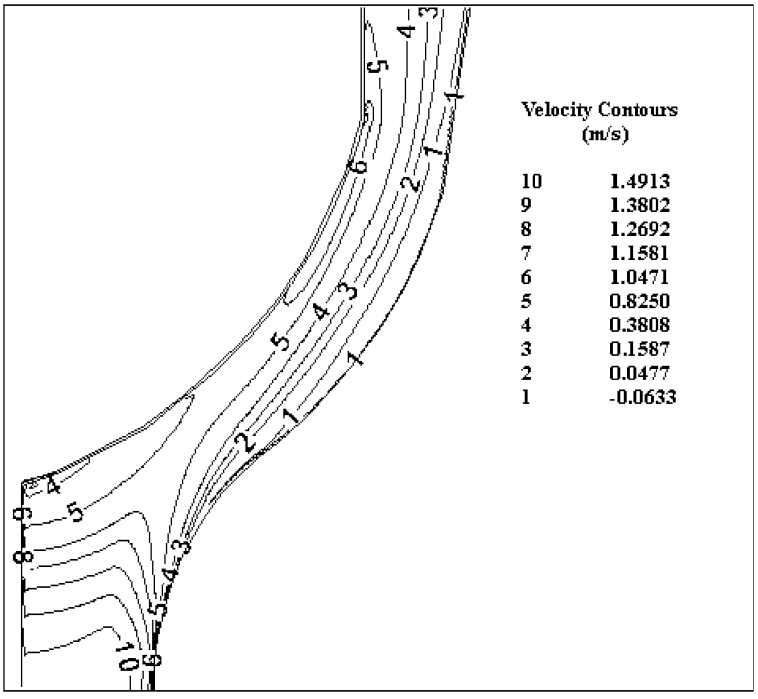

Fig. 16. Window target C3 velocity contours (mass flow rate = 120 kg/s, plasma power = 22.0 kW, inlet temperature 493 K, T91 window with varying thickness from 3 mm on sides to 1.5 mm in the center of window).

voltage than the nozzle anode. The torch is now raised to the pre specified stand off and arc is stabilized. Both the main and the pilot arcs are powered using a 150 kV A (300 V OCV, 500 A) Auto Data make current regulated DC power supply. Both argon and mixed gases like $Ar + N_2$ and $Ar + H_2$ were introduced as plasma generat-

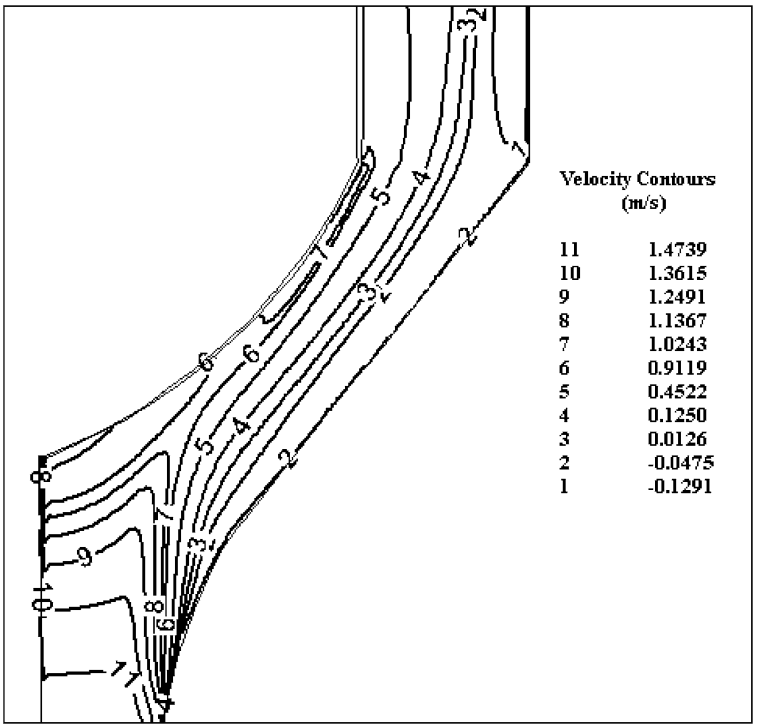

Fig. 17. Window target C4 velocity contours (mass flow rate = 120 kg/s, plasma power = 22.0 kW, inlet temperature 493 K, T91 window with varying thickness from 3 mm on sides to 1.5 mm in the center of window).

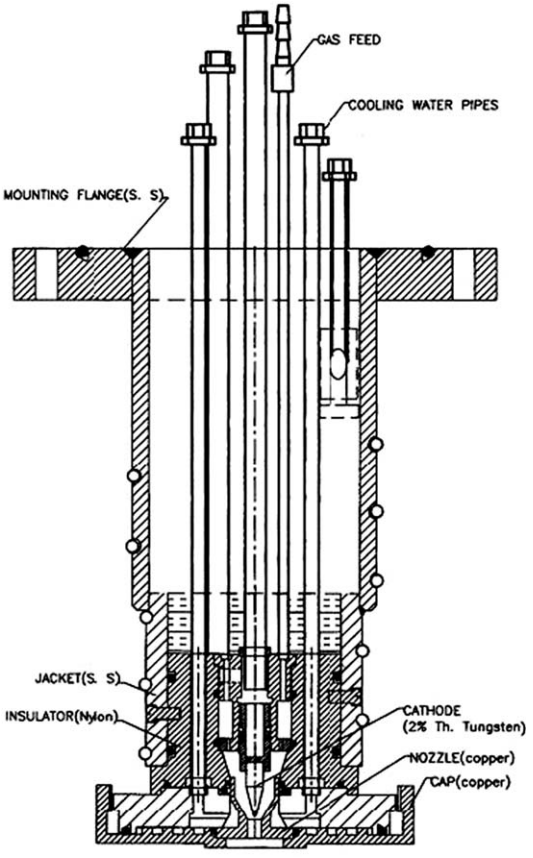

Fig. 18. Details of plasma torch which simulates proton beam heating of window.

ing gases. After the arc is stabilized, heat fluxes at varying flow rates, arc current and torch-substrate (window simulator) standoff distances were measured. A rotating magnetic field of average value between 1 G and 10 G was applied in a direction perpendicular to the arc current lines at the window simulator. This resulted in deflection and rotation of the arc attachment point on the substrate resulting in broadening the heat flux profile delivered to the window simulator. The B field configuration was set up using three solenoid electromagnets (1000-A turn coils) wound on water-cooled mild steel tubes. The electromagnets were located 120° apart and powered from a variac in star connection. In transferred arc mode the magnetic field could spread the arc onto the entire window surface. The heat flux values at the copper window and the SS disc end were then input to a computer code specially developed to invert the data to obtain heat source profile.

Some of the significant conclusions drawn from the plasma runs are the following: There was no undue thermal stress on the torch body or the enclosing tube. The cooling of about 40–50 LPM was adequate. Application of B field reduced peak heat fluxes by 30% and uniform heat flux was achieved at the central window region. The results are summarized in Table 7.

The heat fluxes necessary for ADS target thermo hydraulic simulation are possible only by operating the plasma in the transferred arc mode. Operation in non-transferred arc mode will necessitate high currents, better nozzle cooling and larger sized torch. A mixture of argon with hydrogen or nitrogen is necessary to increase the arc

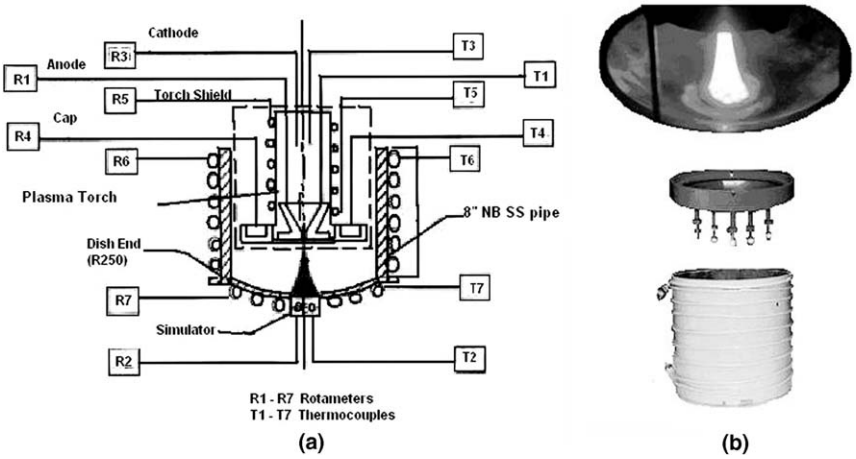

Fig. 19. Schematic and photograph of experimental rig for characterization of plasma torch system for ADS window simulation.

Table 7
Results of various plasma runs to estimate attainable heat flux values

Run No.	Mode (NT/T) non-transferred/ transferred	Arc power – KW (V, A)	Plasma gas (LPM)	Stand off (mm)	Torch efficiency	Surface heat flux (10^4 kW/m^2)
1	NT	9.0 (36 V, 250 A)	Argon (20)	50	43.64	0.051
2	NT	14.0 (40, 350)	Argon (30)	60	45.60	0.072
3	NT	24.8 (62, 400)	Argon (40) N_2 (10)	60	40.0	0.132
4	NT	31.6 (79, 400)	Argon (40) N_2 (20)	50	27.0	0.233
5	T (B = 0)	15.5 (76, 204)	Argon (20)	50	88.2	0.373
5	T (with rotating B field)	26.25 (105, 250)	Argon (20)	80	91.4	0.500
6	T (with rotating B field)	27.75 (111, 250)	Argon (30)	80	92.48	0.505
7	T (with rotating B field)	33.9 (113, 300)	Argon (16)	100	95.80	0.360
8	T (B = 0)	30.5 (122, 250)	Argon (20) H_2 (5)	100	91.01	0.458
9	T (with rotating B field)	36.9 (123, 300)	Argon (20) H_2 (5)	100	91.10	0.548
10	T (with rotating B field)	55.46 (158, 351)	Argon (20) H_2 (5)	160	92.26	0.585
11	T (with rotating B field)	68.00 (170, 400)	Argon (20) H_2 (5)	170	92.45	0.648

voltage and enthalpy. The desired standoff between window and torch may be in the range of 150–200 mm.

6. Summary and conclusion

The design of the spallation target system for ADS requires a deep understanding of the thermal-hydraulic issues involved, as a large amount of heat is deposited by the high energy proton beam both in the circulating LBE target and the window. This necessitates detailed studies with heat simulation. An experimental LBE loop (with a 1:1 size of the actual target) is proposed for simulating the window thermal load by a high power plasma torch. Various window materials will be studied in this facility. Conjugate heat transfer analysis has been carried out for various window materials, geometry and flow configuration to determine cooling capability of LBE. Based on this analysis, a plasma torch has been designed, fabricated and tested. The measured heat fluxes delivered by the torch matched with the required values for the proton beam heat simulation of the window. Using this torch, experiments will be carried out, once the LBE loop is ready. The window configurations and flow geometry studied here will be used for designing the LBE experimental loop. These experiments will give deep insight into the capability of the molten target in extracting the window heating and thus paving the way for designing the LBE target for ADS.

References

[1] C. Rubbia, J.A. Rubia, S. Buono, F. Carminati, N. Fietier, J. Galvez, Y. Kadi, R. Klapisch, P. Mandrillon, J.P. Revol, Ch. Roche, CERN – Group conceptual design of a fast neutron operated high power energy amplifier, Accelerator Driven Systems: Energy Generation and Transmutation of Nuclear Waste, IAEA-TECDOC-985, Vienna, 1997, pp. 187–312.

[2] H. Ait Abderrahim, P. Kupschus, E. Malambu, P.H. Benoit, K. Van Tichelen, B. Arien, F. Kermeersch, P. D'Hondt, Y. Jongen, S. Ternier, D. Vanderplassche, MYRRHA – A multipurpose Accelerator Driven System for Research and Development, IAEA-TECDOC-1356, Moscow, 2003, pp. 71–80.

[3] C. Aragonese, S. Buono, G. Fotia, L. Maciocco, V. Moreau, L. Sorrentino, Review and application to windowless spallation targets of free surface flow models in commercial codes, CRS4 Technical Report 99/20, Italy, 2000, pp. 1–28.

[4] C.H. Lefhalm, J.U. Knebel, K.J. Mack, Kinetics of gas phase oxygen control system (OCS) for stagnant and flowing Pb–Bi systems, Int. J. Nucl. Mater. 296 (2001) 301–304.

[5] V. Bellucci, S. Buono, G. Fotia, L. Maciocco, V. Moreau, M. Mulas, G. Siddi, L. Sorrentino, Requirements of the beam target of the energy amplifier prototype, CRS4-TECH-Rep, 98/38, Center for Advanced Studies, Research and Development in Sardinia, Cagliari, Italy, 2000.
[6] V. Mantha, D. Dutta, T.K. Das, R. Chaudhary, K. Kumar, A.K. Mohanty, P. Satyamurthy, S. Kailas, Thermal-hydraulic analysis of LBE neutron spallation target for ADS, in: P. Singh, L.M. Pant (Eds.), Proceedings of the DAE-BRNS National Symposium on Nuclear Physics, Banaras Hindu University, Varanasi, India, 2004, pp. 582–583.
[7] P. Satyamurthy, K. Biswas, Design of a LBE spallation target for the fast-thermal accelerator driven sub-critical system (ADS), in: L. Echavarri (Ed.), Seventh Information Exchange Meeting, OECD-IAEA-NEA, Jeju, Republic of Korea, 2002, pp. 647–656.
[8] E.J. Weinberg, D.L. Nordstrom, Passage of particles through matter, Phys. Rev. D 54 (1996) 132–139.
[9] P.S.S. Murty, S.N. Sahasrabudhe, N.S. Dixit, S. Ghorui, P. Satyamurthy, A.K. Das, A DC arc plasma beam source for thermal hydraulic simulation of target – proton beam interaction for accelerator driven subcritical systems, in: A.K. Das, A.V. Bapat, A.K. Sinha (Eds.), DAE-BRNS National Symposium on Applications of Plasmas, Lasers, Electron Beams in Advanced Material Processing, BARC, Mumbai, INDIA, 2002, pp. 433–437.
[10] S. Buono, C. Rubbia, A comparison of different materials for the beam window of the energy amplifier, CERN/ET Internal Note, CERN, Geneva, August 1996, pp. 96–26.
[11] B.E. Launder, D.B. Spalding, The numerical computation of turbulent flows, Int. J. Comput. Meth. Appl. Mech. Eng. 3 (1974) 269–289.
[12] R.B. Bird, W.E. Stewart, E.N. Lightfoot, Transport Phenomena, Wiley International Edition, New York, 1960, pp. 85.
[13] H.K. Versteeg, W. Malalasekera, An Introduction to Computational Fluid Dynamics the Finite Volume Method, first ed., Prentice Hall, Pearson Education Limited, Harlow, England, 1995, pp. 67–74.
[14] S. Buono, Review of the thermal and physical properties of Pb-Bi and other heavy liquid metals, in: S. Buono (Ed.), In the First Meeting of the Benchmark Working group on heavy liquid Metal Thermal Hydraulics, Centre for Advanced studies, Research and Development, Sardinia, CRS4, C.P. 94, 09010 UTA, Cagliari, Italy, pp. 10–26.
[15] A.N. Brooks, T.J.R. Hughes, Streamline upwind/Petro–Galkerin formulation for convection dominated flow with particular emphasis on the incompressible Navier–Stokes equations, Int. J. Comput. Meth. Appl. Mech. Eng. 32 (1982) 199–256.
[16] S.V. Patankar, Numerical Heat Transfer and Fluid Flow, first ed., Hemisphere, Washington, DC, 1980, pp. 126–131.
[17] J.G. Rice, R.T. Schnipke, An equal order velocity pressure formulation that does not exhibit spurious pressure modes, Int. J. Comput. Meth. Appl. Mech. Eng. 58 (1986) 135–149.
[18] B.F. Armaly, F. Durst, J.C.F. Perreira, B. Schonung, Experimental and theoretical investigation of backward-facing step flow, J. Fluid Mech. 127 (1983) 473–496.
[19] G. de Vahl Davis, I.P. Jones, Natural convection in a square cavity: a comparison exercise, Int. J. Numer. Meth. Fluids 3 (1983) 249–264.
[20] H. Schlichting, K. Gersten, Boundary Layer Theory, eight ed., Springer-Verlag, Berlin, 2000, pp. 43, 110, 118, 344, 359.
[21] M.B. Toloczko, M.L. Hamilton, S.A. Maloy, High temperature tensile testing of modified 9Cr–1Mo after irradiation with high energy protons, J. Nucl. Mater. 318 (2003) 200–206.